Noncoherent Reconfigurable Intelligent Surface With Differential Modulation and Reflection Pattern Training

Jun Ino, Hiroki Wakatsuchi, *Member, IEEE*, and Shinya Sugiura, *Senior Member, IEEE*

***Abstract*—In this paper, we propose a novel noncoherent reconfigurable intelligent surface (RIS)-assisted downlink architecture aided by lightweight reflection pattern training as well as noncohererent detection. More specifically, the proposed scheme amalgamates the benefits of reflection pattern training and differential modulation, which operate without any channel estimation in each stage of RIS optimization and data detection, hence combating the delay-induced limitations. The proposed scheme achieves low training complexity and robustness over the channel variation in comparison to the conventional RIS optimization assuming the use of channel state information. We demonstrate that the proposed scheme outperforms the conventional coherent benchmarks.**

***Index Terms*—noncoherent detection, overhead reduction, pattern training, reconfigurable intelligent surface, training.**

I. Introduction

Reconfigurable intelligent surface (RIS) has the exclusive benefits of low-cost passive reflection as a virtual relay node [1–3]. Since millimeter-wave communication suffers from the blockage of an obstacle due to its high path loss and low refraction capability, the RIS technology may be a promising solution to extend the coverage in a reliable manner. By contrast, one of the most challenging issues for the practical RIS operation is the substantial overhead needed for controlling the RIS elements as well as the associated increased communication latency [3–5]. To achieve optimal phase shifts of each RIS element, perfect channel state information (CSI) between a base station (BS) and the RIS, as well as that between the RIS and a user, is needed in addition to complicated non-convex optimization based on the acquired CSI. Furthermore, the CSI estimation with pilot transmissions, as well as the non-convex optimization, has to be completed sufficiently faster than channel coherence time. Note that the associated overhead and latency increase upon increasing the number of RIS elements.

In order to relax the limitations imposed by channel estimation and non-convex optimization, several beam-training schemes were proposed for reducing overhead imposed by an RIS control [6–8]. In [7], hierarchical training was proposed, where wide and narrow beam sectors are selected in order. Also, in [8], the complexity imposed by RIS training is reduced with the aid of a multi-mode grouping method that supports moderate combining gain. Alternatively, random RIS beamforming [9] allows us to dispense with CSI knowledge, although the full RIS beamforming gain is unachievable. More recently, in [10, 11], the RIS that is controlled by the pulse width of an incoming wave is proposed to remove the control voltage lines to each RIS element and symbol-level synchronization between the BS and the RIS.

While the majority of the previous RIS studies assumed the coherent detection at the receiver, several RIS-assisted systems employed noncoherent detection [12–14], in order to dispense with the channel estimation and reduce the pilot overhead. In [12], the combination of differential modulation and permutation modulation is exploited at the RIS for a downlink scenario, and the receiver is allowed to detect the signal in a noncoherent manner. In [14], RIS-aided noncoherent OFDM uplink is considered, where differential modulation is employed at an uplink user while RIS relies on random phase reflection at each element. However, the previous noncoherent RIS schemes, such as [12–14], sacrifice the beneficial beamforming gain since associated CSI is unavailable to dispense with channel estimation. More recently, in [15], the combination of differential modulation at a user and beam training of RIS is proposed for an RIS-assisted uplink system, although the presence of the direct user-to-BS link is assumed.[1]

Against the above-mentioned background, the novel contribution of this paper is that we propose the noncoherent RIS-assisted downlink architecture in the absence of an idealistic direct BS-to-user link, in order to dispense with channel estimation for both RIS optimization and data detection.[2] More specifically, the proposed scheme amalgamates the benefits of differential modulation and pattern training, which operate without any channel estimation. The proposed scheme achieves low training complexity and robustness over the channel variation. We demonstrate the performance analysis of the proposed scheme in comparison to the conventional coherent counterpart.

The remainder of this paper is organized as follows. In Section II, we introduce the system model of our RIS-assisted noncoherent communication system. In Section III, our simulation results of the achievable BER performance are provided. Finally, in Section IV, this paper is concluded.

J. Ino and S. Sugiura are with the Institute of Industrial Science, The University of Tokyo, Tokyo 153-8505, Japan (e-mail: sugiura@iis.u-tokyo.ac.jp). (*Corresponding author: Shinya Sugiura.*)

H. Wakatsuchi is with the Graduate School of Engineering, Nagoya Institute of Technology, Nagoya, Aichi 466-8555, Japan.

This work was supported in part by the Japan Society for the Promotion of Science (JSPS) KAKENHI (Grant Number 21H01324, 23H00470), and in part by National Institute of Information and Communications Technology (NICT), Japan.

[1] Most recently, in [16], the tradeoff between the outdatedness of CSI and the system performance is characterized by the effective capacity. Furthermore, in [17], pilot overhead for estimation of uplink cascaded channel is reduced in a sub-6-GHz scenario.

[2] In a millimeter-wave scenario, an RIS is typically expected to combat the detrimental non-line-of-sight scenario (NLOS) while RIS does not have to be activated in the presence of a stable direct link.

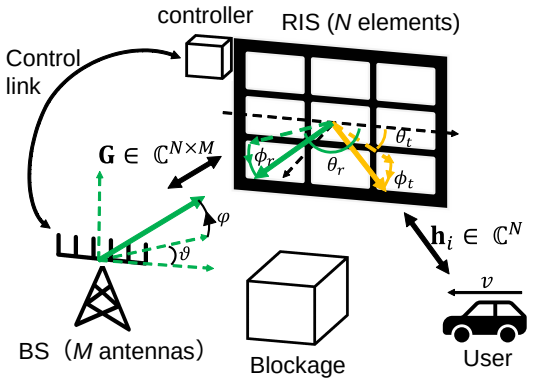

Fig. 1. System model of our noncoherent RIS scheme.

II. System Model

In this section, we present the channel model considered in this paper. Then, our reduced-overhead RIS-assisted architecture and its noncoherent detection are proposed.

A. Channel Model

We consider a downlink communication scenario, where a single BS, an RIS, and a single-antenna user equipment (UE) are supported, as shown in Fig. 1. The BS is equipped with a uniform linear array (ULA) with M antenna elements, which is placed along the x-axis, and the spacing between adjacent antenna elements is given by d_{B}. The RIS consists of a uniform rectangular array with N passive reflecting elements, which is installed perpendicular to the xy plane. Hence, we denote N_x and N_z as the number of RIS elements along the x-axis and the z-axis, respectively, hence having $N = N_x N_z$. The separations of the RIS elements in the x- and z-directions are given by d_x^{R} and d_z^{R}, respectively. We assume that the RIS is controlled by a dedicated controller connected to the BS with a high-speed, reliable optical link. The link between the BS and the RIS and that between the RIS and the UE are modeled as Rice fading, which is typically considered for millimeter-wave communications [18]. Also, we assume that the channels between the BS and the RIS are constant while the channels between the RIS and the UE are affected by the Doppler effect similar to [3]. Furthermore, the BS communicates with the UE via the RIS in the absence of a direct link.

Channel coefficients between the BS and the RIS $\mathbf{G} \in \mathbb{C}^{N\times M}$ and those between the RIS and the UE in the ith time index $\mathbf{h}_i = [h_1^{(i)}, \cdots, h_N^{(i)}]^T \in \mathbb{C}^N$ are represented, respectively, by [15]

$$\mathbf{G} = \sqrt{\frac{L_{\mathrm{BR}}}{\kappa_{\mathrm{BR}}+1}}\left(\sqrt{\kappa_{\mathrm{BR}}}\bar{\mathbf{G}} + \tilde{\mathbf{G}}\right) \tag{1}$$

$$\mathbf{h}_i = \sqrt{\frac{L_{\mathrm{RU}}}{\kappa_{\mathrm{RU}}+1}}\left(\sqrt{\kappa_{\mathrm{RU}}}\bar{\mathbf{h}}_i + \tilde{\mathbf{h}}_i\right), \tag{2}$$

where L_{BR} and L_{RU} are the associated large-scale fading coefficients, while κ_{BR} and κ_{RU} are the corresponding Rice factors. Furthermore, $\bar{\mathbf{G}}$ and $\tilde{\mathbf{G}}$ denote the line-of-sight (LOS) and NLOS components for the link between the BS and the RIS. Similarly, $\bar{\mathbf{h}}_i$ and $\tilde{\mathbf{h}}_i$ correspond to the LOS and NLOS components for the link between the RIS and the UE. Hence, the ith symbol sampled at the user is given by

$$y_i = \underbrace{\mathbf{h}_i^T \mathbf{\Omega}\mathbf{G}\mathbf{w}}_{c_i} x_i + n_i \in \mathbb{C} \quad (i \geq 1), \tag{3}$$

where $\mathbf{w} \in \mathbb{C}^M$ represent the antenna weights at the BS, having the power constraint of $\|\mathbf{w}\|^2 = P_t$, and P_t denotes the BS transmit power. Also, x_i is an information symbol, and n_i represents the additive white Gaussian noise (AWGN) component with the zero mean and a variance of σ^2. Furthermore, $\mathbf{\Omega} \in \mathbb{C}^{N\times N}$ is a diagonal matrix, whose nth entry represents the reflection coefficient of the nth RIS element ($1 \leq n \leq N$), and we have $\boldsymbol{\omega} = [\omega_1 \cdots, \omega_N]^T = \mathrm{diag}[\mathbf{\Omega}] \in \mathbb{C}^N$. Then, the cascaded end-to-end channel coefficient is defined by $c_i = \mathbf{h}_i^T \mathbf{\Omega}\mathbf{G}\mathbf{w} \in \mathbb{C}$.

Moreover, according to Clarke's model [3], the NLOS components of the channels between the RIS and the UE $\tilde{\mathbf{h}}_i$ are modeled by the random variables obeying complex-valued Gaussian distribution $\mathcal{CN}(0,1)$ with the zero mean and a unit variance under the correlation of

$$\mathbb{E}\left[\tilde{h}_n^{(l)}(\tilde{h}_n^{(m)})^*\right] = J_0\left(2\pi f_d |l-m|\right). \tag{4}$$

Here, $\mathbb{E}[\cdot]$ is the expectation operation and J_0 represents the first-order Bessel function. Furthermore, f_d is the normalized maximum Doppler frequency. The NLOS components of the channels between the BS and the RIS $\tilde{\mathbf{G}}$ are modeled by the random variables of $\mathcal{CN}(0,1)$.

By contrast, the geometric channel model [6] is employed for characterizing each LOS component as follows:

$$\bar{\mathbf{G}} = \mathbf{a}_{\mathrm{B}}^T(\vartheta,\varphi) \otimes \mathbf{a}_{\mathrm{R}}(\theta^r,\phi^r) \tag{5}$$

$$\bar{\mathbf{h}}_i = \exp(j2\pi i f_d \cos\theta_t)\mathbf{b}_{\mathrm{R}}(\theta^t,\, \phi^t), \tag{6}$$

where $\mathbf{a}_{\mathrm{R}}(\theta^r,\phi^r) \in \mathbb{C}^N$ denotes a receive array response vector at the RIS, while $\theta^r \in [0,\pi]$ and $\phi^r \in [-\pi/2.\pi/2]$ are the azimuth and elevation angle-of-arrival (AoAs) from the BS to the RIS. Similarly, $\mathbf{a}_{\mathrm{B}}(\vartheta,\varphi) \in \mathbb{C}^M$ and $\mathbf{b}_{\mathrm{R}}(\theta^t,\phi^t) \in \mathbb{C}^M$ are the transmit array responses at the BS and the RIS, respectively, where $\vartheta \in [0,\pi]$ and $\varphi \in [-\pi/2,\pi/2]$ denote azimuth and elevation angles-of-departure (AoDs) from the BS, while $\theta^t \in [0,\pi]$ and $\phi^t \in [-\pi/2,\pi/2]$ are the azimuth and elevation AoDs from the RIS to the user. Also, $\otimes$ denotes the Kronecker product.

Furthermore, the array response vectors of $\mathbf{a}_{\mathrm{B}}(\vartheta,\varphi)$, $\mathbf{a}_{\mathrm{R}}(\theta^r,\phi^r)$, and $\mathbf{b}_{\mathrm{R}}(\theta^t,\phi^t)$ may be rewritten by

$$\mathbf{a}_{\mathrm{B}}(\vartheta,\varphi) = \mathbf{u}(\psi_{\mathrm{B}}^t, M) \tag{7}$$

$$\mathbf{a}_{\mathrm{R}}(\theta^r,\phi^r) = \mathbf{u}(\psi_{\mathrm{R},x}^r, N_x) \otimes \mathbf{u}(\psi_{\mathrm{R},z}^r, N_z) \tag{8}$$

$$\mathbf{b}_{\mathrm{R}}(\theta^t,\phi^t) = \mathbf{u}(\psi_{\mathrm{R},x}^t, N_x) \otimes \mathbf{u}(\psi_{\mathrm{R},z}^t, N_z) \tag{9}$$

where

$$\mathbf{u}(\psi,i) = [1, e^{-j\psi\pi}, e^{-j2\psi\pi}, ..., e^{-j(i-1)\psi\pi}]^T, \tag{10}$$

while we have

$$\psi_{\mathrm{B}}^{t} = \frac{2d_{\mathrm{B}}}{\lambda}\cos\vartheta\cos\varphi \tag{11}$$

$$\psi_{\mathrm{R},x}^{r} = \frac{2d_{x}^{\mathrm{R}}}{\lambda}\cos\theta^{r}\cos\phi^{r} \tag{12}$$

$$\psi_{\mathrm{R},z}^{r} = \frac{2d_{z}^{\mathrm{R}}}{\lambda}\sin\phi^{r} \tag{13}$$

$$\psi_{\mathrm{R},x}^{t} = \frac{2d_{x}^{\mathrm{R}}}{\lambda}\cos\theta^{t}\cos\phi^{t} \tag{14}$$

$$\psi_{\mathrm{R},z}^{t} = \frac{2d_{z}^{\mathrm{R}}}{\lambda}\sin\phi^{t}. \tag{15}$$

Also, λ represents the wavelength.

We assume that the BS and the RIS remain unmoved, and the LOS component associated with the channel between them is considered quasi-static. Hence, the beam at the BS is fixed toward RIS to maximize the received LOS component at the RIS by setting the antenna weights to be $\mathbf{w} = \sqrt{P_t/M}\mathbf{a}_{\mathrm{B}}^{*}(\vartheta,\varphi)$.

Furthermore, the fixed BS weights allow us to simplify the cascaded channel as follows. First, let us define the LOS component of the cascaded channel $\bar{c}_i$ as

$$\bar{c}_i = \eta\bar{\mathbf{h}}_i^{T}\mathbf{\Omega}\bar{\mathbf{G}}\mathbf{w}, \tag{16}$$

where

$$\eta = \sqrt{\frac{L_{\mathrm{BR}}\kappa_{\mathrm{BR}}}{(\kappa_{\mathrm{BR}}+1)}}\sqrt{\frac{L_{\mathrm{RU}}\kappa_{\mathrm{RU}}}{(\kappa_{\mathrm{RU}}+1)}}. \tag{17}$$

Also, in the rest of this paper, $\mathbf{u}(\psi_{\mathrm{R},x}^{t}, N_x)$ and $\mathbf{u}(\psi_{\mathrm{R},z}^{t}, N_z)$ are simply expressed as $\mathbf{u}(\psi_{\mathrm{R},x}^{t})$ and $\mathbf{u}(\psi_{\mathrm{R},z}^{t})$, respectively. Then, $\bar{c}_i$ is represented by [6]

$$\bar{c}_i = \eta\bar{\mathbf{h}}_i^{T}\mathbf{\Omega}\bar{\mathbf{G}}\mathbf{w} \tag{18}$$

$$= \eta\sqrt{P_t/M}\bar{\mathbf{h}}_i^{T}\mathbf{\Omega}(\mathbf{a}_{\mathrm{B}}^{H}(\vartheta,\varphi)\mathbf{a}_{\mathrm{B}}(\vartheta,\varphi))\mathbf{a}_{\mathrm{R}}(\theta^{r},\phi^{r}) \tag{19}$$

$$= \lambda_i\sqrt{P_tM}\mathbf{b}_{\mathrm{R}}^{T}(\theta^{t},\phi^{t})\mathbf{\Omega}\mathbf{a}_{\mathrm{R}}(\theta^{r},\phi^{r})$$

$$= \lambda_i\sqrt{P_tM}(\mathbf{u}(\psi_{\mathrm{R},x}^{t})\otimes\mathbf{u}(\psi_{\mathrm{R},z}^{t}))\odot(\mathbf{u}(\psi_{\mathrm{R},x}^{r})\otimes\mathbf{u}(\psi_{\mathrm{R},z}^{r}))\boldsymbol{\omega}$$

$$= \lambda_i\sqrt{P_tM}(\mathbf{v}_x^{T}\otimes\mathbf{v}_z^{T})\boldsymbol{\omega}, \tag{20}$$

where

$$\lambda_i = \exp(j2\pi i f_d\cos\theta_t)\eta \tag{21}$$

$$\mathbf{v}_x = \mathbf{u}(\psi_{\mathrm{R},x}^{t})\odot\mathbf{u}(\psi_{\mathrm{R},x}^{r}) \tag{22}$$

$$\mathbf{v}_z = \mathbf{u}(\psi_{\mathrm{R},z}^{t})\odot\mathbf{u}(\psi_{\mathrm{R},z}^{r}), \tag{23}$$

and $\odot$ denotes the Hadamard product.

According to [6], the constraint of $\boldsymbol{\omega} = \boldsymbol{\omega}_x\otimes\boldsymbol{\omega}_z$ is imposed, where $\boldsymbol{\omega}_x \in \mathbb{C}^{N_x}$ and $\boldsymbol{\omega}_z \in \mathbb{C}^{N_z}$ are decomposed RIS's array steering vectors in the x axis and in the z axis, respectively. Then, (20) is rewritten by

$$\bar{c}_i = \lambda_i\sqrt{P_tM}(\mathbf{v}_x^{T}\otimes\mathbf{v}_z^{T})(\boldsymbol{\omega}_x\otimes\boldsymbol{\omega}_z) \tag{24}$$

$$= \lambda_i\sqrt{P_tM}(\mathbf{v}_x^{T}\boldsymbol{\omega}_x)(\mathbf{v}_z^{T}\boldsymbol{\omega}_z) \tag{25}$$

By setting $\boldsymbol{\omega}_x = \mathbf{v}_x^{*}/\|\mathbf{v}_x\|$ and $\boldsymbol{\omega}_z = \mathbf{v}_z^{*}/\|\mathbf{v}_z\|$, $|\bar{c}_i|$ is maximized to $\eta\sqrt{P_tM}\|\mathbf{v}_x\|\|\mathbf{v}_z\|$. As shown in (25), the trained horizontal (x-axis) and vertical (z-axis) RIS patterns are decoupled. Hence, by assuming that $\phi^{t} = 0$ is set and known by the BS, we can focus our attention on the horizontal-pattern training, similar to [6].

B. Reflection Pattern Training

Our RIS optimization consists of two steps, i.e., offline pattern design and online pattern training. More specifically, we prepare T RIS reflection patterns offline, i.e., in advance of transmissions. A minimum correlation of each pattern pair is minimized under the condition that minimum reflection gain to all reflected directions is kept higher than a specific threshold. Note that employing a low T value results in broad patterns.

In the proposed reflection pattern training scheme, one out of T RIS reflection patterns is selected. More specifically, the BS periodically transmits T reference symbols to the UE via the RIS while changing the reflection patterns of the RIS in each symbol interval. Then, based on feedback information, the BS finally determines the best reflection pattern that achieves the highest received power at the UE.

The conventional narrow-beam training of the RIS reflection coefficients training, which is based on exhaustive search, requires high pilot overhead, depending on the beam resolution [19]. Since the RIS is typically equipped with a large number of reflective elements, i.e., $N \gg 1$, the training overhead of the exhaustive search becomes significantly high. In order to circumvent this limitation, our proposed scheme exploits wide beam training with low training overhead $T \ll N$ at the expense of the reduction in the received power at the user.

More specifically, the ith RIS reflection pattern ($1 \le i \le T$) is designed for configuring a beam covering $\theta^{t} \in [\pi(i-1)/T, \pi i/T]$.

C. Differential Modulation and Noncoherent Detection

Having attained the BS weights and the RIS reflection coefficients above, now data transmission employing differential modulation at the BS is introduced. This allows us to eliminate CSI estimation at the user not only at the optimization stage of the RIS coefficients but also for data detection. At the BS, information bits are modulated onto the phase-shift keying (PSK) symbols s_t ($t \ge 1$), which are then differentially modulated as follows: [20]

$$x_t = \begin{cases} s_0 & t = 1 \\ x_{t-1}s_{t-1} & t \ge 2 \end{cases}, \tag{26}$$

where s_0 is a reference symbol transmitted at the beginning of data transmission.

From (26) and (3), we obtain

$$y_{i+1} = y_i s_i + n_{i+1} - n_i s_i \quad (i \ge 1), \tag{27}$$

under the assumption that the cascaded channel remains unchanged over the intervals of two symbols. Finally, the information symbols are detected based on the maximum likelihood detection as follows:

$$\hat{s}_i = \arg\min_{\forall s} |y_{i+1} - y_i s|^2 \quad (i \ge 1). \tag{28}$$

D. Overhead and Complexity Analysis

In this section, we characterize the pilot overhead and the complexity imposed for calculating the RIS coefficients

TABLE I
COMPARISONS OF PILOT OVERHEAD AND RIS OPTIMIZATION COMPLEXITY BETWEEN THE PROPOSED AND BENCHMARK SCHEMES

	Pilot overhead and delay per coherent time	Complexity
Proposed training-based algorithm	$\mathcal{O}(T)$	$\mathcal{O}(T)$
CSI-based (AO) algorithm [22]	$\mathcal{O}(N)$	$\mathcal{O}(M^3+N^{3.5})$

in the proposed scheme. Here, we consider the benchmark scheme that estimates N cascaded channels by sending N pilot symbols while changing the RIS activation patterns. The comparisons are listed in Table I.

In the proposed scheme, the RIS pattern optimization is carried out every T pilot transmission, while the conventional scheme typically requires N full pilot transmissions. Hence, in the proposed scheme, decreasing the T value contributes to the reduction of the pilot overhead and the delay, which are imposed by the RIS pattern control. By contrast, in the conventional CSI-based RIS control, non-convex optimization is carried out based on the estimated CSI. However, since the original rate-maximization problem of an RIS-assisted communication scenario is typically non-convex, obtaining the optimal solution is a challenging task [21]. Also, even in the sub-optimal solution based on alternating optimization [22], it imposes the complexity order of $\mathcal{O}(M^3+N^{3.5})$.

Furthermore, note that pilot symbols are inserted within every coherent interval in the conventional scheme, the associated pilot overhead, delay, and complexity increase upon increasing the channel's time variation.

III. PERFORMANCE RESULTS

In this section, we provide our performance results to demonstrate the achievable performance of the proposed scheme. The conventional full-RIS optimization based on pilot-assisted CSI estimation is employed as a benchmark. The basic system parameters are selected as follows. A carrier frequency and a symbol rate are set to 30 GHz and 120 kHz, respectively. The RIS is placed horizontally on the x-axis from point $(5,5,0)$ m. The ULA at the BS is equipped with $M=8$ antenna elements, which are placed along the x-axis from the origin point. We assume that the user is randomly located within a semicircle with a radius of $\sqrt{50}$ m from the RIS. Large-scale fading coefficients are given by

$$L_{\rm BR} = \xi_0 (d_{\rm BR}/d_0)^{\gamma_{\rm BR}} \tag{29}$$

$$L_{\rm RU} = \xi_0 (d_{\rm RU}/d_0)^{\gamma_{\rm RU}}, \tag{30}$$

where $d_{\rm BR}$ and $d_{\rm RU}$ denote the distance between the BS and the RIS and that between the RIS and the user while ξ is a reference gain normalized for the distance of $d_0=1$ m. Note that, in this paper, the average SNR is defined as [6]

$$\text{SNR} = \frac{P_t L_{\rm BR} L_{\rm RU} N^2 M}{\sigma^2}, \tag{31}$$

where P_t is the transmit power at the BS. In our simulations, we employed $\xi_0 = -62$ dB, $\gamma_{\rm BR} = -2.3$, $\gamma_{\rm RU} = -2$, and $\sigma^2 = -105$ dBm.

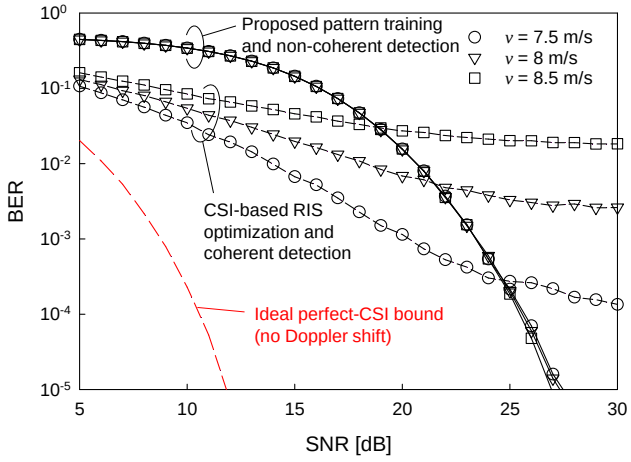

Fig. 2. BER comparisons between the proposed scheme and the benchmark schemes. We consider the system parameters of $(N,T)=(16,4)$, and the Rice factor of each link is set to $\kappa_{\rm BR}=\kappa_{\rm RU}=10$ dB. The velocity of the UE is given by $v=7.5$, 8, and 8.5 m/s.

Fig. 2 shows the achievable BER performance of the proposed and benchmark schemes, where v is varied from 7.5 to 8.5 m/s, while we have the system parameters of $(N,T)=(16,4)$. Also, we consider $\kappa_{\rm BR}=\kappa_{\rm RU}=10$ dB. We also plotted the idealistic bound with no Doppler shift, where perfect CSI is used for the RIS optimization and coherent detection. For the benchmark scheme, the block length is set to 34, and 16 pilot symbols are inserted at the beginning of each block. Observe in Fig. 2 that regardless of the v value, the proposed scheme achieved successful error-floor-free curves. By contrast, the benchmark scheme suffers from the error floor, whose level increases upon increasing v due to the effects of the Doppler shift, where the RIS optimization, as well as the coherent detection, is carried out based on the outdated channel estimation. More importantly, the proposed scheme reduced the pilot overhead by a factor of 25% in comparison to the RIS pattern-training scheme.

Fig. 3 shows the BERs of the proposed scheme, where the number of training patterns was given by $T=2,4,8$, and 16, where we have $v=10$ m/s. Observe in Fig. 3 that the BER performance monotonically improves upon increasing the T value. More specifically, the SNR recorded for the BER of 10^{-4} with $T=4$ exhibited 6-dB gain over that of $T=2$. This is because the high number of training patterns allows us to have the high reflected beamforming gain at the sacrifice of increased overhead and delay.

Furthermore, Fig. 4 shows the BERs of the proposed scheme, where the Rice factor was varied from -10 dB to 5 dB, while maintaining $\kappa_{\rm BR}=\kappa_{\rm RU}$. Also, we consider $v=10$ m/s. It was found that upon increasing the Rice factor, the BER performance improved. This is achieved owing to our system architecture, which is designed for millimeter wave scenarios where the LOS paths are dominant.

Additionally, while our focus in this paper is on a single-user scenario, the proposed scheme is readily applicable to multiuser scenarios, similar to conventional wireless sys-

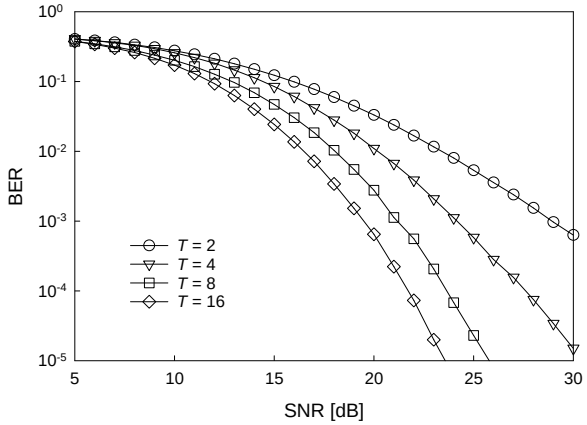

Fig. 3. BER performance of the proposed scheme, where the number of training symbol intervals is given by $T = 2$, 4, 8, and 16, while we have $N = 16$ and $v = 10$ m/s. The Rice factor of each link is set to $\kappa_{\mathrm{BR}} = \kappa_{\mathrm{RU}} = 5$ dB.

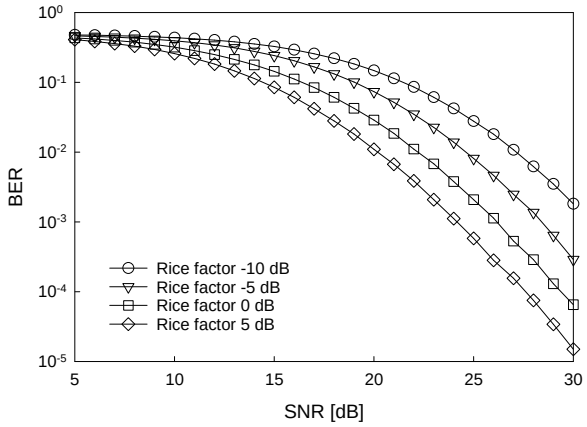

Fig. 4. BER performance of the proposed scheme, where the Rice factor of each link is given by $\kappa_{\mathrm{BR}} = \kappa_{\mathrm{RU}} = -10$ dB, -5 dB, 0 dB, and 5 dB, while we have $v = 10$ m/s.

tems. For example, our RIS system can be straightforwardly employed in time-division multiple access (TDMA) and frequency-division multiple access (FDMA) scenarios.

IV. Conclusions

In this paper, we proposed the novel RIS-assisted noncoherent downlink communication scheme. Owing to our amalgamation of CSI-free RIS pattern training and differential coding with noncoherent detection, the RIS control and data communication are accomplished with reduced pilot overhead. Our performance results demonstrated that the proposed scheme outperforms the conventional benchmarks that require channel estimation and non-convex optimization in terms of BER performance.

References

[1] S. Sugiura, Y. Kawai, T. Matsui, T. Lee, and H. Iizuka, "Joint beam and polarization forming of intelligent reflecting surfaces for wireless communications," *IEEE Transactions on Vehicular Technology*, vol. 70, no. 2, pp. 1648–1657, 2021.

[2] C. Xu, J. An, T. Bai, L. Xiang, S. Sugiura, R. G. Maunder, L.-L. Yang, and L. Hanzo, "Reconfigurable intelligent surface assisted multi-carrier wireless systems for doubly selective high-mobility Ricean channels," *IEEE Transactions on Vehicular Technology*, vol. 71, no. 4, pp. 4023–4041, 2022.

[3] C. Xu, J. An, T. Bai, S. Sugiura, R. G. Maunder, Z. Wang, L.-L. Yang, and L. Hanzo, "Channel estimation for reconfigurable intelligent surface assisted high-mobility wireless systems," *IEEE Transactions on Vehicular Technology*, vol. 72, no. 1, pp. 718–734, 2023.

[4] B. Zheng, C. You, W. Mei, and R. Zhang, "A survey on channel estimation and practical passive beamforming design for intelligent reflecting surface aided wireless communications," *IEEE Communications Surveys & Tutorials*, vol. 24, no. 2, pp. 1035–1071, 2022.

[5] S. Noh, J. Lee, G. Lee, K. Seo, Y. Sung, and H. Yu, "Channel estimation techniques for RIS-assisted communication: Millimeter-wave and sub-THz systems," *IEEE Vehicular Technology Magazine*, vol. 17, no. 2, pp. 64–73, 2022.

[6] C. You, B. Zheng, and R. Zhang, "Fast beam training for IRS-assisted multiuser communications," *IEEE Wireless Communications Letters*, vol. 9, no. 11, pp. 1845–1849, 2020.

[7] B. Ning, Z. Chen, W. Chen, Y. Du, and J. Fang, "Terahertz multi-user massive MIMO with intelligent reflecting surface: Beam training and hybrid beamforming," *IEEE Transactions on Vehicular Technology*, vol. 70, no. 2, pp. 1376–1393, 2021.

[8] R. Singh and B. Kumbhani, "How to train intelligent reflecting surfaces?" *IEEE Communications Letters*, vol. 26, no. 8, pp. 1923–1927, 2022.

[9] Q. Tao, S. Zhang, C. Zhong, and R. Zhang, "Intelligent reflecting surface aided multicasting with random passive beamforming," *IEEE Wireless Communications Letters*, vol. 10, no. 1, pp. 92–96, 2021.

[10] A. A. Fathnan, H. Homma, S. Sugiura, and H. Wakatsuchi, "Method for extracting the equivalent admittance from time-varying metasurfaces and its application to self-tuned spatiotemporal wave manipulation," *Journal of Physics D: Applied Physics*, vol. 55, no. 1, p. 015304, 2022.

[11] A. A. Fathnan, K. Takimoto, M. Tanikawa, K. Nakamura, S. Sugiura, and H. Wakatsuchi, "Unsynchronized reconfigurable intelligent surfaces with pulse-width-based design," *IEEE Transactions on Vehicular Technology*, pp. 1–6, 2023, in press.

[12] S. Guo, J. Ye, P. Zhang, H. Zhang, and M.-S. Alouini, "Differential reflecting modulation for reconfigurable intelligent surface-based communications," *IEEE Communications Letters*, vol. 25, no. 3, pp. 907–910, 2021.

[13] H. Ma, Y. Fang, P. Chen, and Y. Li, "Reconfigurable intelligent surface-aided m-ary FM-DCSK system: A new design for noncoherent chaos-based communication," *IEEE Transactions on Vehicular Technology*, pp. 1–15, 2022, DOI: 10.1109/TVT.2022.3226749, in press.

[14] K. Chen-Hu, G. C. Alexandropoulos, and A. G. Armada, "Non-coherent modulation for RIS-empowered multi-antenna OFDM communications," *arXiv*, 2021, cs.IT, 2103.05547.

[15] K. Chen-Hu, G. C. Alexandropoulos, and A. g. Armada, "Differential data-aided beam training for RIS-empowered multi-antenna communications," *IEEE Access*, vol. 10, pp. 113 200–113 213, 2022.

[16] S. W. Haider Shah, S. Pavan Deram, and J. Widmer, "On the effective capacity of RIS-enabled mmWave networks with outdated CSI," in *IEEE INFOCOM*, York City, NY, USA, Aug. 2023, pp. 1–10.

[17] H. Guo and V. K. N. Lau, "Uplink cascaded channel estimation for intelligent reflecting surface assisted multiuser MISO systems," *IEEE Transactions on Signal Processing*, vol. 70, pp. 3964–3977, 2022.

[18] J. Huang, C.-X. Wang, Y. Sun, R. Feng, J. Huang, B. Guo, Z. Zhong, and T. J. Cui, "Reconfigurable intelligent surfaces: Channel characterization and modeling," *Proceedings of the IEEE*, vol. 110, no. 9, pp. 1290–1311, 2022.

[19] C. Qi, K. Chen, O. A. Dobre, and G. Y. Li, "Hierarchical codebook-based multiuser beam training for millimeter wave massive MIMO," *IEEE Transactions on Wireless Communications*, vol. 19, no. 12, pp. 8142–8152, 2020.

[20] C. Xu, N. Ishikawa, R. Rajashekar, S. Sugiura, R. G. Maunder, Z. Wang, L.-L. Yang, and L. Hanzo, "Sixty years of coherent versus non-coherent tradeoffs and the road from 5G to wireless futures," *IEEE Access*, vol. 7, pp. 178 246–178 299, 2019.

[21] Q. Wu, S. Zhang, B. Zheng, C. You, and R. Zhang, "Intelligent reflecting surface-aided wireless communications: A tutorial," *IEEE Transactions on Communications*, vol. 69, no. 5, pp. 3313–3351, 2021.

[22] Q. Wu and R. Zhang, "Intelligent reflecting surface enhanced wireless network via joint active and passive beamforming," *IEEE Transactions on Wireless Communications*, vol. 18, no. 11, pp. 5394–5409, 2019.